



## Article

# Modeling and Control of a Soft Robotic Arm Based on a Fractional Order Control Approach

Carlos Relano <sup>1,\*</sup> , Jorge Muñoz <sup>1</sup> , Concepción A. Monje <sup>1</sup> , Santiago Martínez <sup>1</sup> and Daniel González <sup>2</sup><sup>1</sup> Robotics Lab, Carlos III University of Madrid, Avda de la Universidad 30, 28911 Leganés, Spain<sup>2</sup> Arquimea Aerospace Defence and Security, Calle Margarita Salas 10, 28919 Leganés, Spain

\* Correspondence: crelano@ing.uc3m.es

**Abstract:** Controlling soft robots is a significant challenge due to the nonlinear elastic nature of the soft materials that conform their structure. This paper studies the identification and control problems of a novel two-degrees-of-freedom, tendon-actuated, soft robotic arm. A decoupled identification approach is presented; later, a fractional order control strategy is proposed and tested experimentally, in comparison with PI solutions. The simulation and experimental results show the goodness of the modeling and control approaches discussed.

**Keywords:** soft robotics; fractional order control; modeling of soft robots; control of soft robots

## 1. Introduction

One of the main objectives of robotics is to create universal and adaptable machines capable of performing a variety of tasks and proactively adapting to changing conditions. While conventional robots are able to perform specific tasks with exceptional precision, speed or reliability, they find significant difficulties in adapting to other more compliant tasks as well as in operating in completely unstructured environments.

To overcome these difficulties, the new field of soft robotics has emerged, where soft elements are used to replace rigid robotic links and joints. The softness of these robots is a promising feature for improving interaction with the environment. When comparing the degrees of freedom (DoF) of a rigid manipulator versus a soft manipulator, it is observed that rigid robots move in 6 DoF (position and orientation), while soft bodies have an infinite number of DoF [1]. This feature provides them with capabilities such as adaptability and better shock absorption.

Since soft robotics is a new, innovative and very active field of research, new designs and methods of operation are continuously emerging. However, with such different platforms and their unique attributes, it is difficult to find integrative methodologies for their modeling and control [2].

Deformations of soft robots are difficult to predict, and actuators are often integrated into the structure, resulting in a coupled actuation [3]. Soft materials also exhibit nonlinearities such as compliance and hysteresis, which restrict high-frequency control. Conventional control approaches assume the stiffness of the robot links, and when translated directly to the control of robots with soft links, they do not adapt well. Therefore, new control algorithms are required when working with soft robotics [4,5].

Concerning soft robot control, two approaches are mainly used: open loop control and closed loop control. For the open loop approach, the most common technique used is the finite element method (FEM) [6]. This method approximates the continuous deformation of the system. For instance, in [3], a real-time FEM control model for a pneumatic robotic manipulator is proposed. However, due to its high computational cost, FEM is often used for offline validation of analytical models and experimental results [7]. The closed loop (feedback) allows the correction of control inaccuracies due to external agents and model



**Citation:** Relano, C.; Muñoz, J.; Monje, C.A.; Martínez, S.; González, D. Modeling and Control of a Soft Robotic Arm Based on a Fractional Order Control Approach. *Fractal Fract.* **2023**, *7*, 8. <https://doi.org/10.3390/fractalfract7010008>

Academic Editor: Saptarshi Das

Received: 21 October 2022

Revised: 26 November 2022

Accepted: 16 December 2022

Published: 22 December 2022



**Copyright:** © 2022 by the authors. Licensee MDPI, Basel, Switzerland. This article is an open access article distributed under the terms and conditions of the Creative Commons Attribution (CC BY) license (<https://creativecommons.org/licenses/by/4.0/>).

uncertainties. Nevertheless, a suitable model is also very important in this case in order to find a suitable controller. The soft robot's high complexity makes empirical or tuning rules ineffective in this case. Two different approaches can be found in the literature for closed loop control: the first focuses on the control of a soft actuator and the second focuses on the control of the complete robot structure, which integrates all actuators and soft links. For instance, some actuator control examples can be found in the control of dielectric elastomers [8], twisted and coiled polymers [9], or shape memory alloys [10]. In this paper, we apply the second approach.

A greater number of different methodologies are found in the control of the complete soft system. Some examples are the use of model predictive control (MPC) together with a simplified physical model of the joint space of a pneumatic soft robotic arm [11]; the soft robotic arm driven by 12 wires embedded inside a silicon body made at the BioRobotics Institute of Pisa, which uses a Proportional Integral Derivative (PID) control [12]; or the soft robotic neck driven by three wires made at the RoboticsLab of the University Carlos III of Madrid, which uses a fractional order controller (FOC) [13]. From these control techniques, fractional order controllers have demonstrated to be a good alternative to their integer order versions [14]. Nevertheless, control remains one of the main challenges in soft robotics.

Fractional order controllers allow the exponents of the integral and derivative actions to be noninteger (fractional). This way, besides the three proportional ( $k_p$ ), integral ( $k_i$ ) and derivative ( $k_d$ ) parameters defining the integer PID, a fractional order PID (FOPID) introduces two other parameters into the tuning process: the orders of the integral ( $\lambda$ ) and derivative ( $\mu$ ) operations, respectively. This order generalization allows a higher number of control specifications to be met and a wider variety of controller design methods, from optimization to more intuitive graphical approaches [15].

The features provided by fractional order control are useful for controlling the dynamics of soft robotic systems where robustness and precision are important. Different combinations of control actions can be selected according to each particular control problem. For instance, an example of the potential of using a fractional order PI (FOPI) for the control of a soft link is presented in [16], where a robust pose performance is obtained. The control problem when using a fractional order PD (FOPD) for the case of a soft robotic neck is also addressed in [17].

The aim of this paper is to develop a functional controller for the soft robotic arm shown in Figure 1, developed at the RoboticsLab of the Universidad Carlos III of Madrid (see [18] for details). Its innovative design is under a patenting process [19]. The arm acts by means of a central soft element made up of NinjaFlex (thermoplastic polyurethane), which allows the flexion in two axes of rotation thanks to the tension produced by three tendons attached to the tip of the robot.

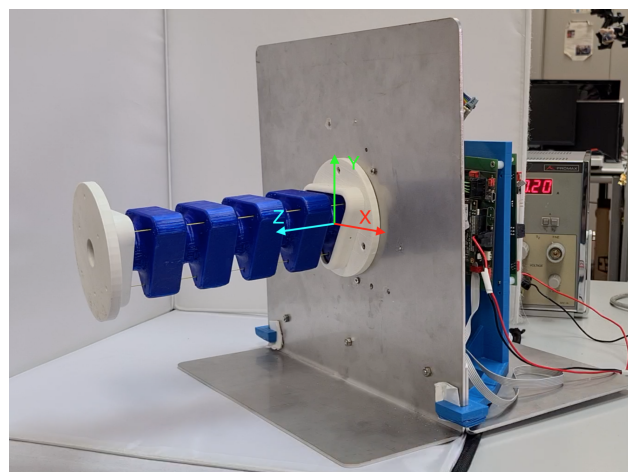


Figure 1. Soft robotic arm platform.

In [18], an open loop actuation was performed on the soft arm using a kinematic approach. However, using an open loop configuration makes it difficult to perform accurate positioning and to respond to changes in the system, such as external loads. Since precision is one of the most difficult goals in soft robotics, it is important to find an improvement in control. Given the soft characteristics of the arm, when high loads are applied, it may bend excessively. This is a challenge to be faced from the control side, which will be responsible for limiting this extra bending while ensuring accurate positioning.

From these results, the need to use a closed loop configuration becomes clear. PID controllers are one of the most widespread control methodologies; over 95% of control loops are PI/PID type [20]. This is due to advantages such as their simple implementation and the large number of tuning methods that are available and proving to be very useful for a multitude of systems. However, this simplicity may become a disadvantage when the system requires more demanding control constraints. When trying to control the soft arm under certain conditions, the response may not be stable.

Therefore, a fractional order controller is proposed for the closed loop control of this innovative soft arm, which presents different morphological characteristics with respect to other soft robot designs. Designing, prototyping and controlling this robot are very challenging problems not previously faced in the literature; this work addresses them all at once and contributes to soft robotics real-world applications, and also to the experimental application of fractional order controllers.

From the system identification perspective, a new methodology for decoupling the soft robot model is presented, which allows decomposing the system into a simpler set of subsystems. From the control system perspective, we propose a fractional order controller and demonstrate experimentally how the generalization of a robust controller as the PI into its fractional order version makes it possible to address the very challenging control problems that arise from the soft nature of the robot.

The rest of the paper is organized as follows. Section 2 presents a detailed description of the soft arm platform and its operation. Section 3 describes the mathematical methodology to deal with the modeling and decoupling of the system. Section 4 details the methodology used for the system identification, and Section 5 describes the selection of the control specifications and development of the controllers. Section 6 analyses the results, comparing the data obtained from real experiments using different controllers and loads. Finally, Section 7 summarizes the main conclusions of the work.

## 2. Description of the Soft Arm Platform

The actuation of the soft robotic arm (Figure 1) is achieved by varying the length of each of the three tendons placed longitudinally inside its link. The tendons are routed through the vertices of the triangles and are attached to the free end of the arm and to a winch at the base. A motor is responsible for the pulling of each tendon and, therefore, for the bending of the arm.

Unlike other designs that commonly have a cylindrical shape [21,22], this design has a triangular morphology that allows different locking configurations. As shown in Figure 2a,b, the maximum curvature is different when bending in the direction of the triangle vertices than when bending in the direction of the triangle edges. This property can be used for the protection of the structure when heavy loads are placed at the tip or when a high flexion of the arm is demanded, which can compromise the integrity of the robot. In addition, the configurations can be used as locks to help prevent the movement of load [19].

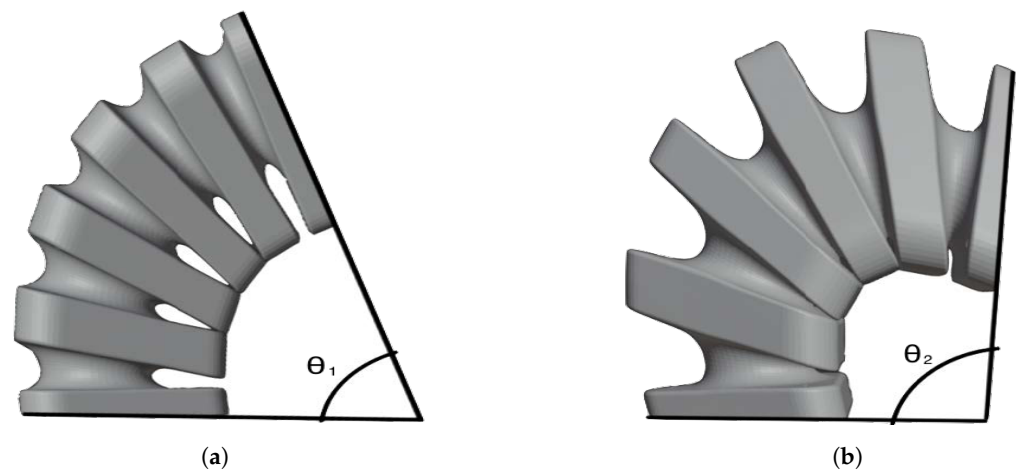


**Figure 2.** Comparing panels (a,b), the maximum curvatures in the different directions of the soft arm show that angle  $\theta_2$  is greater than angle  $\theta_1$ . (a) Maximum curvature of the soft arm, angle  $\theta_1$ , when bending in the direction of the vertices. (b) Maximum curvature of the soft arm, angle  $\theta_2$ , when bending in the direction of the edges.

The initial length of the tendons is considered equal to the height of the soft arm, which is 0.2 m in this design. These lengths are modified by the winding or unwinding of the tendon as it rotates through the actuation of the motor, a Maxon EC-max 22. The motors are controlled by Technosoft's Intelligent Drives iPOS 4808 MX. The combination of tendon lengths provides different tip positions. The tendons are numbered and arranged for identification: tendon 1 is positioned on the Y-axis; tendons 2 and 3 are named counterclockwise,  $120^\circ$  apart from each other, at a distance  $a$  from the center of the triangle, as shown in Figure 3.

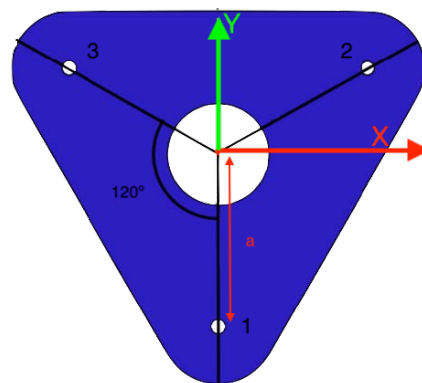


**Figure 3.** Description of tendon distribution in the soft arm.

The orientation of the end-effector, in a three-dimensional environment, can be defined by the combination of the three Euler angles. In this case, Roll—the rotation defined by the Z-axis—cannot change. Data are obtained from the inertial measurement unit (IMU) (sensor 3DM-GX5-10) placed at the top of the arm. Therefore, the final orientation can be described as the combination of Pitch and Yaw, these being the rotation angles around the X and Y axis, respectively, as illustrated in Figure 4a,b.

Therefore, the soft arm can be considered as a multiple-input multiple-output (MIMO) system with three inputs and two outputs. The inputs are the lengths of the tendons, which are controlled by motors, and the outputs are the pitch and yaw angles, which are measured by the IMU.

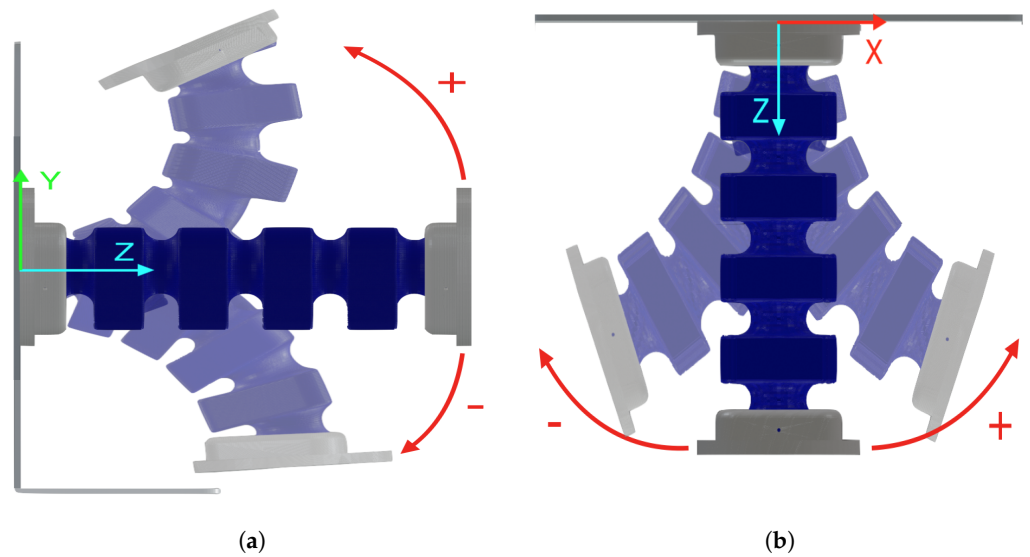


**Figure 4.** The panels show the flexion of the soft robotic arm (a) from a lateral view in positive and negative pitch flexion and (b) from a top view in positive and negative yaw flexion. For a negative pitch bending, panel (a) shows how the vertices will touch, preventing further bending in that direction. For a positive pitch flexion, the edges need more bending for this contact to occur. The yaw flexion in panel (b) has symmetry in the positive and negative directions. The combination of pitch and yaw rotations allows movements with two degrees of freedom, and the limits of flexion vary according to the combined rotations.

### 3. Modeling Approach

For modeling of the robotic system, a decoupling method is proposed so that the MIMO system can be modeled as two independent SISO subsystems by addressing the kinematic problem separately for the pitch ( $\alpha$ ) and yaw ( $\beta$ ) movements. These two new subsystems are more easily identifiable, allowing us to obtain the transfer functions  $G_a(s)$  and  $G_b(s)$  for  $\alpha$  and  $\beta$ , respectively.

To decouple the systems, as explained in [16], the angle  $\alpha$  is described by the following equation:

$$\alpha_i = \cos(\gamma_i)f(L_i) \quad (1)$$

where  $\alpha_i$  is the angle contribution of each actuator to the final angle around the X-axis,  $\gamma_i$  is the projection factor that depends on the relative angle of each actuator,  $L_i$  is the variation of the initial length of each tendon and  $f$  is a nonlinear function that describes the relationship between them. Using the above methodology, a similar equation can be formulated for  $\beta_i$  as the angle contribution of each actuator to the final angle around the Y-axis:

$$\beta_i = \sin(\gamma_i)f(L_i) \quad (2)$$

The resulting tip angles depend on the forces produced by the linear actuators. Therefore, given the construction of the robot, although the  $f$ -functions are nonlinear, the angles can be considered additive, resulting in the following Equations (1) and (2):

$$\alpha = \alpha_1 + \alpha_2 + \alpha_3 =$$

$$\cos(\gamma_1)f(L_1) + \cos(\gamma_2)f(L_2) + \cos(\gamma_3)f(L_3) \quad (3)$$

$$\beta = \beta_1 + \beta_2 + \beta_3 =$$

$$\sin(\gamma_1)f(L_1) + \sin(\gamma_2)f(L_2) + \sin(\gamma_3)f(L_3) \quad (4)$$

Equations (3) and (4) consider the same distribution of the actuators, and the values of  $\gamma_i$  for this specific case are  $\gamma_1 = 0^\circ$ ,  $\gamma_2 = 120^\circ$  and  $\gamma_3 = 240^\circ$ . Therefore, the equations can be rewritten as

$$\alpha = f(L_1) - 0.5 \cdot f(L_2) - 0.5 \cdot f(L_3) = f(L_1) - 0.5 \cdot [f(L_2) + f(L_3)] \quad (5)$$

$$\beta = 0 \cdot f(L_1) + 0.866 \cdot f(L_2) - 0.866 \cdot f(L_3) = 0.866 \cdot [f(L_2) - f(L_3)] \quad (6)$$

Angles  $\alpha$  and  $\beta$  depend on the difference in tendon length. Besides, as the same type of actuator is used for each tendon, it can be assumed that the functions  $f$  relating the actuator angle and the variation of each tendon length are also similar. Based on this, variables  $\alpha$  and  $\beta$  can be redefined as a linear combination of the tendon lengths without loss of generality. In addition, it can be observed that, when acting in  $\beta$ , the tendon length  $L_1$ s has no influence on the movement, and for  $L_1 = L_2 = L_3 = 0$ , angles  $\alpha$  and  $\beta$  are 0 and the length of the soft arm  $l$  is the length of the tendons at rest (no flexion).

Taking into account this redefinition of  $\alpha$  and  $\beta$ , the variations in the tendon lengths can be calculated from Equations (5) and (6) as follows:

$$L_1 = \alpha + 0.5 \cdot [L_2 + L_3] \quad (7)$$

$$L_2 = \frac{\beta}{0.866} + L_3 \quad (8)$$

$$L_3 = -\frac{\beta}{0.866} + L_2 \quad (9)$$

The results of Equations (7)–(9) are a system of three unknowns— $L_1, L_2, L_3$ —and two equations, since Equations (8) and (9) are the same equation. It is then assumed that, during flexion, the curvature is constant. The assumption of constant curvature means that the entire arm will have the same angle of curvature while performing, as occurs in the arc of a circle. Considering the assumption of a constant curvature for this tendon distribution, the following Equation (10) can be used [23], obtaining the third equation for the three unknowns system, where the three unknowns can be related:

$$l = \frac{l_1 + l_2 + l_3}{3} = l + \frac{L_1 + L_2 + L_3}{3} \quad (10)$$

where  $l_i$  is the length of the tendon with constant curvature and  $l_i = l + L_i$ ; consequently,  $L_1 + L_2 + L_3 = 0$ . By solving this system of equations, the resulting tendon lengths as a function of angles  $\alpha$  and  $\beta$  are

$$L_1 = \frac{\alpha}{1.5} \quad (11)$$

$$L_2 = \frac{\beta}{1.732} - \frac{\alpha}{3} \quad (12)$$

$$L_3 = -\frac{\beta}{1.732} - \frac{\alpha}{3} \quad (13)$$

In summary, through the decoupling process, the relationship between the tendon lengths and angles  $\alpha$  and  $\beta$  has been obtained (Equations (11)–(13)). Lengths  $L_i$  will be the references to be achieved by the motors when acting to reach a pose given by the pair  $(\alpha, \beta)$ .

Although an important nonlinear behavior is expected due to the system and material properties, as observed in other experiments [16], it is the aim to propose a robust control strategy based on FOC to overcome these modeling mismatches and achieve a good arm performance. It is worth mentioning that our arm design approaches constant curvature performance, and this assumption allows a significant simplification of the system model versus others that require numerous parameters to be estimated and a high computational cost when it comes to control [2].

#### 4. System Identification

This section describes the methodology used to identify the two SISO subsystems addressed in the previous section. The identification is achieved through the two transfer functions  $G_a(s)$  and  $G_b(s)$  introduced before, which are linear functions that use the Laplace transform to represent the dynamic and stationary behaviors of any system.

The real data used for the identification process are the velocities commanding the motors (system inputs) and the pitch and yaw angles or the arm measured by the IMU (system outputs).

The reason behind the use of a velocity input model is the asymmetry of the pitch performance and the gravity effect. As discussed above, seen from the YZ plane (Figure 4a), a positive pitch movement is achieved by the actuation of two tendons, which are closer to the central bending axis of the soft arm, whereas a negative pitch is achieved by the other tendon further away from the bending axis. When a motor position input is used for the identification, the system presents a strong asymmetry with respect to the positive and negative pitch values  $\alpha$  achieved, as shown in Figure 5. The data show a nonlinear behavior that makes it impossible to formulate just one transfer function to represent the system model for the whole pitch range. This problem is avoided when using a motor velocity input, as will be discussed below, which yields a more consistent behavior in both directions and facilitates both the system identification and the later control problem.

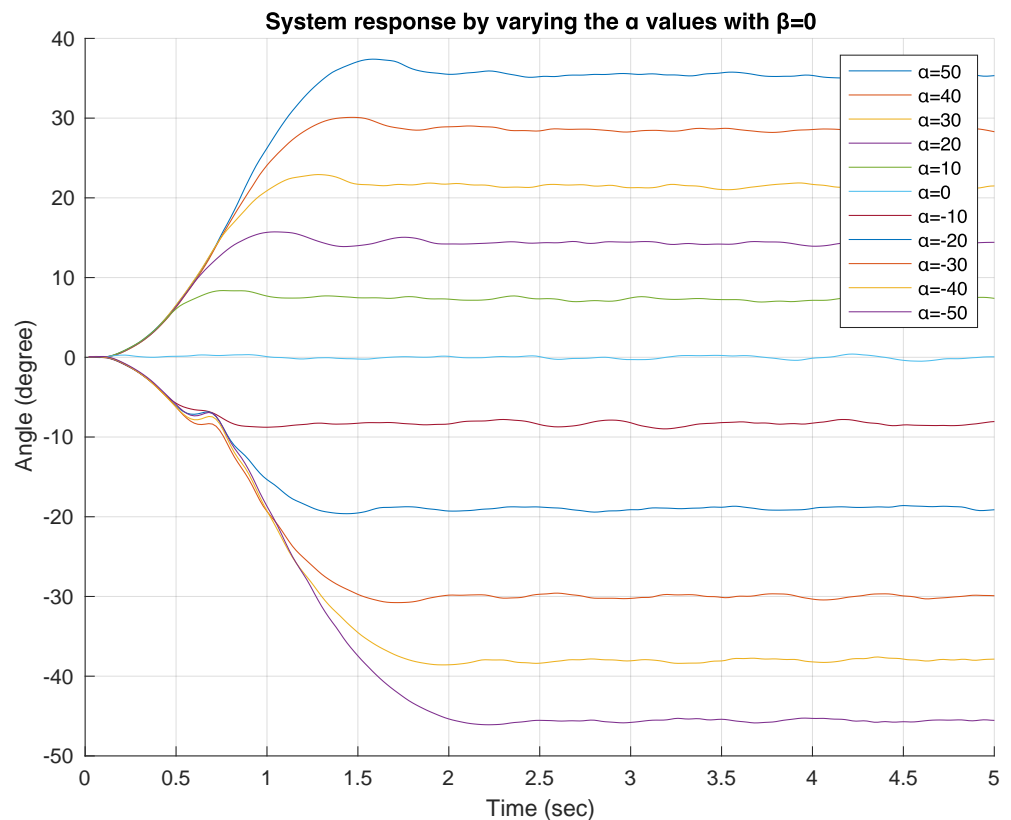


**Figure 5.** Identification data using motor position input and pitch output. Step references for  $\alpha$  within the range  $[-50, 50]$  in steps of 10 degrees with a random  $\pm 1$  noise and with constant  $\beta = 0$  have been used. It can be seen that the pitch position reached in time is different for positive and negative bending.

Therefore, the identification of the systems  $G_a(s)$  and  $G_b(s)$  is now addressed considering the motor angular velocity as input in radians per second, measured by the motor encoders, and the pitch and yaw angles in degrees as outputs, respectively, measured by the IMU. This difference in units has no practical implication other than to increase the gain

of the identified function. Degrees have been chosen for the output for a better visualization of the signal range, and radians per second for the motors because these are the units used by the encoders.

Since this is a system where the input is an angular velocity and the output is an angular position, the identification made is expected to contain an integrator in it. For the identification of each system, a pulse train input alternating every two seconds between the values of 3 and  $-3$  radians per second is used, as shown in Figure 6 for the pitch case. Since an integrator is expected, a step cannot be applied as the bending would grow without limit.

During the identification tests, the variation of the angular position of the arm tip was measured both in pitch and yaw directions. Due to the flexible nature of the arm, a slight vibration occurs in the system when an abrupt change in velocity is applied. This effect is more visible for the pitch case due to the action of gravity, as can be seen in Figure 6. The parameters are initialized through the Instrument Variable (IV) method, and updated by means of a nonlinear least-squares search method [24].

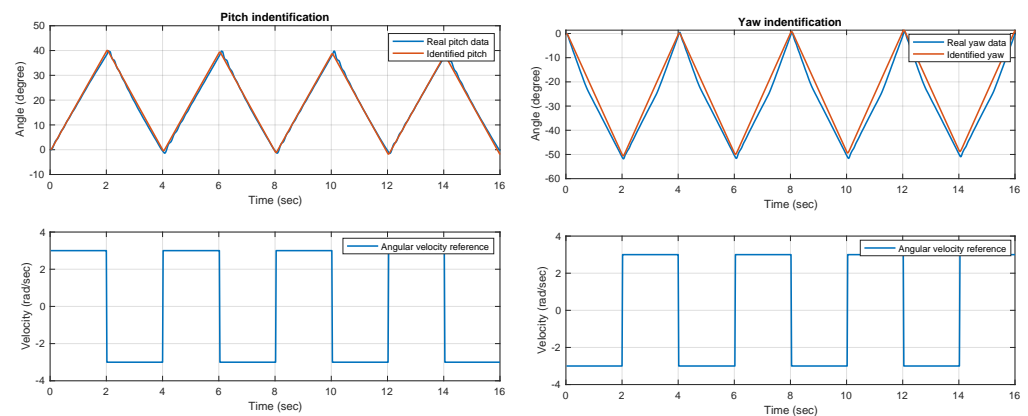


**Figure 6.** Identification data using motor velocity input and pitch (left) and yaw (right) output.

Once the identification data are obtained, the corresponding two transfer functions  $G_a(s)$  and  $G_b(s)$  are identified by defining some parameters such as the number of poles, zeros and delay [25], which yields the following two second-order functions:

$$G_a(s) = \frac{402.41}{(s + 59.33)(s + 0.008883)} \quad (14)$$

$$G_b(s) = \frac{372.2}{(s + 43.51)(s + 0.006044)} \quad (15)$$

As can be observed, both transfer functions have a pole very close to the origin, which represents dynamics similar to an integrator, as expected.

## 5. Control Specification and Tuning

In the following, integer and fractional order control approaches will be discussed and analyzed. PI and FOPI controllers will be addressed. The PI structure has been chosen against the conventional PID due to the fact that the derivative action amplifies the vibration noise of the soft arm, and it is preferable to avoid it. Regarding the design specifications, constraints on the phase margin ( $\phi_m$ ) and the gain crossover frequency ( $\omega_{gc}$ ) of the open loop control system will be imposed. These specifications are chosen because they allow us through the phase margin ( $\phi_m$ ) to act on the damping ratio and through the gain crossover frequency ( $\omega_{gc}$ ) on the speed of the system response and stability.

The design of the PI controllers, which have the transfer function given in Equation (16), has been widely discussed in the control literature [26–28], and there are different methodologies for the tuning of the controller parameters. In this work, the PID Tuning Algorithm

of [20] has been used to obtain the parameters  $k_p$  and  $k_i$  that make it possible for the pitch  $G_a(s)$  and yaw  $G_b(s)$  decoupled systems to fulfill the specifications of phase margin and the gain crossover frequency.

$$C_{PI}(s) = k_p + \frac{k_i}{s} \quad (16)$$

Fractional order controllers rely on the use of noninteger orders (exponents of the integral and derivative operations in the Laplace domain) to achieve design specifications that their integer counterparts cannot meet, allowing the fulfillment of robust performance constraints. In this work, the term robustness is used to refer to the ability to cope with the action of external disturbances or loads that cause unwanted deformations in soft bodies, while providing sufficient accuracy and keeping the overshoot of the response constant to gain changes [15].

Fractional order PID controllers are proposed as a generalization of integer order PID due to the fact that they offer a robust performance against changing plant parameters and nonlinearities, as explained in [29]. As discussed above, the fractional order proportional integral (FOPI) variant of this controller will be used in this case, whose transfer function is

$$C_{FOPI}(s) = k_p + \frac{k_i}{s^\lambda} \quad (17)$$

where  $\lambda$  is the fractional order of the integral operator.

Classic tuning methods cannot be applied for fractional order controllers; therefore, other techniques have been developed such as optimization [30], graphical approaches [31] or others [15]. In this work, the iso-m method [13] will be applied, which allows for controller tuning in a simple and intuitive way while avoiding optimization problems such as local minima or graphical resolution. This approach provides all fractional order controller parameters defined in Equation (17) for specific values of the phase margin and gain crossover frequency, but keeping the open loop system phase flat, thus meeting the desired specifications of stability and responsiveness of the system while providing a robust system performance. In the case of the soft arm, the system itself shows a variable gain during the operation, making the robust controller a need in order to achieve a constant performance for all motions.

In order to analyze and compare the performance of the controllers, tuning with different design conditions will be carried out.

Regarding the variation of the performance speed, this is achieved by the selection of different values of the gain crossover frequency  $\omega_{gc}$ . The bigger the frequency, the faster the system response. Regarding the variation of the soft arm loads, they are expected to affect the nominal model of the system, mainly changing its gain. Therefore, the controller has to perform robustly to gain changes, guaranteeing not only the system stability for the whole gain range but a constant overshoot of the time response, which will limit the undesired bending of the arm when heavy loads are carried.

### 5.1. The First Control Specifications: $\phi_m = 60^\circ$ and $\omega_{gc} = 1.5 \text{ rad/s}$

First, a PI controller is designed for each of the systems  $G_a(s)$  and  $G_b(s)$ , defined in Equations (14) and (15), using the PID tuning method cited before. The resulting controller parameters are shown in Table 1, and their transfer functions are given by Equations (18) and (19), respectively.

**Table 1.** PI controller parameters for  $\phi_m = 60^\circ$  and  $\omega_{gc} = 1.5 \text{ rad/s}$ .

Plant	$k_p$	$k_i$
$G_a(s)$	0.1937	0.1603
$G_b(s)$	0.1546	0.1246

$$C_{PI_a}(s) = 0.1937 + \frac{0.1603}{s} \quad (18)$$

$$C_{PI_\beta}(s) = 0.1546 + \frac{0.1246}{s} \quad (19)$$

Using the same specifications, the corresponding FOPI controllers are also designed using the iso-m tuning method described in [13]. The following operations must be carried out for the iso-m controller tuning for the pitch case:

- Step 1. The system phase and phase slope found at  $\omega_{gc}$  are  $\Phi_s = -91.1deg$  and  $m_s = -4.1deg/\log(\omega)$ , respectively.
- Step 2. The controller is required to contribute with a phase slope opposite to that of the system—that is,  $m = 4.1deg/\log(\omega)$ . Besides, in order to achieve the phase margin specification, the controller has to provide a phase  $\Phi_c = (-(-91.1) + 60 - 180)deg$  at  $\omega_{cg}$ —that is,  $\Phi_c = -28.9deg$ .
- Step 3. Based on these two values from Step 2, the fractional order resulting from the slopes graph available in [13] is  $\alpha = -0.38$ .
- Step 4. Using these values,  $\tau_a$  is computed (see [13] for more details), resulting  $\tau_a = 6.1026$ .
- Step 5. Finally, the controller gain  $k$  is computed, resulting  $k = 0.0361$ .
- Step 6. Therefore, according to the method, the controller parameters are  $k_p = 0.0361$ ,  $k_a = 0.2205$  and  $\alpha = -0.38$ .

Following the same steps, the yaw controller was tuned, obtaining a slightly different result. The corresponding controller parameters are shown in Table 2, and their transfer functions are given by Equations (20) and (21), respectively.

**Table 2.** FOPI controller parameters for  $\phi_m = 60^\circ$  and  $\omega_{gc} = 1.5$  rad/s.

Plant	$k_p$	$k_i$	$\lambda$
$G_a(s)$	0.0361	0.2205	0.3800
$G_b(s)$	0.0361	0.1682	0.3900

$$C_{FOPI_\alpha}(s) = 0.0361 + \frac{0.2205}{s^{0.38}} \quad (20)$$

$$C_{FOPI_\beta}(s) = 0.0361 + \frac{0.1682}{s^{0.39}} \quad (21)$$

An approximation of the fractional order operator  $s^\lambda$  is then needed in order to implement the FOPI controller in the feedback control scheme of the soft arm. One of the most common techniques is the equivalent pole-zero approximation described in [32], based on the operator frequency response (see for example [33]). Using this method, the resulting controller approximations are

$$C_{FOPI_\alpha}^*(s) = \frac{14.24s^3 + 89.98s^2 + 40.91s + 1.583}{s^4 + 140.3s^3 + 362.7s^2 + 70.47s + 0.9836} \quad (22)$$

$$C_{FOPI_\beta}^*(s) = \frac{13.38s^3 + 78.35s^2 + 33.81s + 1.268}{s^4 + 158.8s^3 + 391.7s^2 + 72.29s + 0.9619} \quad (23)$$

### 5.2. The Second Control Specifications: $\phi_m = 60^\circ$ and $\omega_{gc} = 5$ rad/s

These specifications imply a faster system response but keeping a similar overshoot in comparison with the first experiment. Following the previous tuning methods, the resulting PI controller parameters and transfer functions are shown in Table 3 and Equations (24) and (25), respectively; and the resulting FOPI controller parameters and transfer functions are shown in Table 4 and Equations (26), (27), (28) and (29), respectively.

$$C_{PI_\alpha}(s) = 0.6689 + \frac{1.5800}{s} \quad (24)$$

$$C_{PI_\beta}(s) = 0.5395 + \frac{1.1740}{s} \quad (25)$$

$$C_{FOPI\alpha}(s) = 0.3083 + \frac{0.9967}{s^{0.46}} \quad (26)$$

$$C_{FOPI\beta}(s) = 0.3168 + \frac{0.7401}{s^{0.52}} \quad (27)$$

$$C_{FOPI\alpha}^*(s) = \frac{515.2s^3 + 7383s^2 + 9064s + 1060}{s^4 + 1192s^3 + 8329s^2 + 4252s + 151.6} \quad (28)$$

$$C_{FOPI\beta}^*(s) = \frac{717.2s^3 + 7771s^2 + 8203s + 901.6}{s^4 + 1849s^3 + 1.043e04s^2 + 4371s + 125.4} \quad (29)$$

**Table 3.** PI controller parameters for  $\phi_m = 60^\circ$  and  $\omega_{gc} = 5$  rad/s.

Plant	$k_p$	$k_i$
$G_a(s)$	0.6689	1.5800
$G_b(s)$	0.5395	1.1740

**Table 4.** FOPI controller parameters for  $\phi_m = 60^\circ$  and  $\omega_{gc} = 5$  rad/s.

Plant	$k_p$	$k_i$	$\lambda$
$G_a(s)$	0.3083	0.9967	0.4600
$G_b(s)$	0.3168	0.7401	0.5200

## 6. Experimental Results

In this section, the performance of the different controllers proposed will be compared by means of their Bode and time response plots. The purpose is to test the system behavior at different speeds and with different loads placed at its tip. The system robustness will be addressed through a load test consisting of adding a 500 g disc at the tip of the arm.

### 6.1. First Experiment: Using Control Specifications $\phi_m = 60^\circ$ and $\omega_{gc} = 1.5$ rad/s

The Bode plots of the open loop systems with the corresponding PI and FOPI controllers are shown in Figure 7 for the PI case and Figure 8 for the FOPI case.

As can be seen, the phase margin and gain crossover frequency specifications are met in all cases. However, regarding the robustness of the system, the effect of the iso-damping property can be clearly observed in the Bode phase curves of the systems with the FOPI controllers. A flat phase around the gain crossover frequency has been forced, ensuring that variations in the gain of the system will not significantly affect the phase margin and, therefore, achieving a constant overshoot.

Tests are carried out on the real system with the proposed controllers, testing the time response to a pitch step reference of  $\alpha = 40^\circ$  and keeping a constant yaw angle of  $\beta = 0^\circ$ . Figures 9 and 10 show the ideal time response represented as the dashed red line, the experimental response of the system without load as the blue continuous line and the experimental response with a load of 500 g as the orange continuous line.

Tables 5 and 6 show the response metrics of the systems with and without loads for the PI and FOPI controllers, respectively. Data related to the peak value, peak time and overshoot are presented together with the value of the root mean square error (RMSE) during the first 8 s of the response calculated as

$$\text{RMSE} = \sqrt{\frac{\sum_{i=1}^N (\hat{y}_i - y_i)^2}{N}} \quad (30)$$

where  $\hat{y}_i$  is the ideal response at sample  $i$ ,  $y_i$  is the corresponding experimental response and  $N = 400$  samples (8 s at 50 Hz). In addition, settling times of  $t_s = 4.55$  s and  $t_s = 5.31$  s have been obtained for the PI and FOPI cases, respectively.

Even if the system performance is robust for both control approaches and only slight differences can be noticed, it is remarkable that the overshoot for the FOPI case (15.1% for simulation test) is smaller and its variation is also more constrained than for the PI case (23.8% for simulation test).

In order to test the system performance under more demanding speed and trajectory conditions, a second experiment will be carried out, as described in the following section.

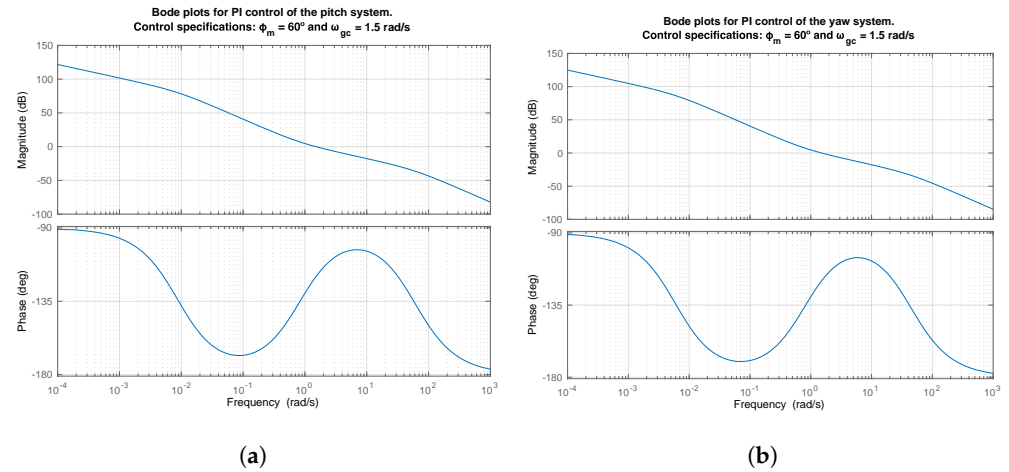


**Figure 7.** Bode plots of the open loop systems with the resulting PI controllers. Control specifications:  $\phi_m = 60^\circ$  and  $\omega_{gc} = 1.5$  rad/s. (a) Bode plots of the open loop system with the PI controller corresponding to the pitch system. (b) Bode plots of the open loop system with the PI controller corresponding to the yaw system.

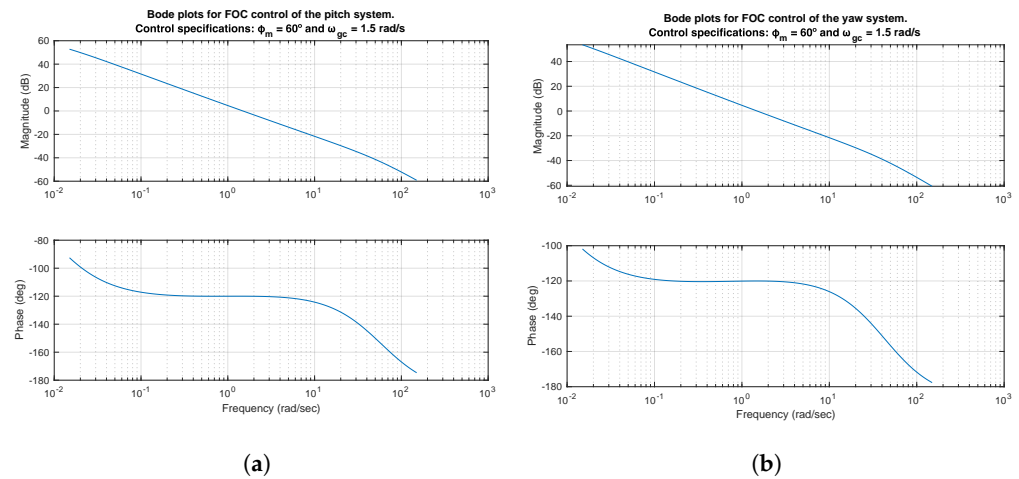


**Figure 8.** Bode plots of the open loop systems with the resulting FOPI controllers. Control specifications:  $\phi_m = 60^\circ$  and  $\omega_{gc} = 1.5$  rad/s. (a) Bode plots of the open loop system with the FOPI controller corresponding to the pitch system. (b) Bode plots of the open loop system with the FOPI controller corresponding to the yaw system.

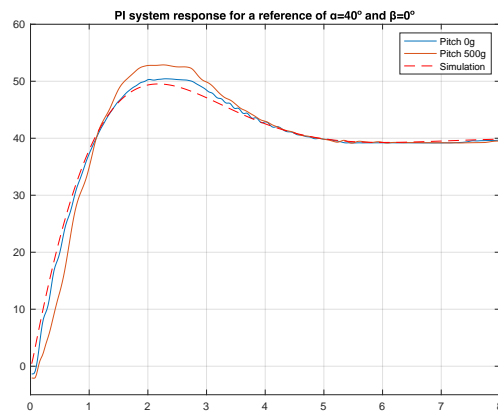


**Figure 9.** System response with the PI controller for a pitch step reference of  $\alpha = 40^\circ$  and a constant yaw angle of  $\beta = 0^\circ$ . Control specifications:  $\phi_m = 60^\circ$  and  $\omega_{gc} = 1.5$  rad/s.

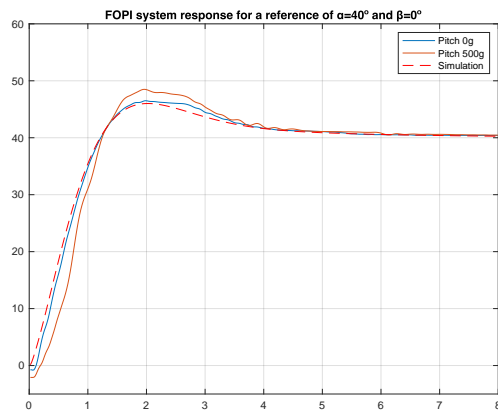


**Figure 10.** System response with the FOPI controller for a pitch step reference of  $\alpha = 40^\circ$  and a constant yaw angle of  $\beta = 0^\circ$ . Control specifications:  $\phi_m = 60^\circ$  and  $\omega_{gc} = 1.5$  rad/s.

**Table 5.** PI system response. Control specifications:  $\phi_m = 60^\circ$  and  $\omega_{gc} = 1.5$  rad/s.

Data	Peak Value (deg)	Peak Time (s)	Overshoot (%)	RMSE
Simulation	49.5	2.2	23.8%	-
PI: 0 g	50.4337	2.3	26.0842%	0.9765
PI: 500 g	52.8717	2.26	32.1794%	2.9153

**Table 6.** FOPI system response. Control specifications:  $\phi_m = 60^\circ$  and  $\omega_{gc} = 1.5$  rad/s.

Data	Peak Value (deg)	Peak Time (s)	Overshoot (%)	RMSE
Simulation	46	2.05	15.1%	-
FOPI: 0 g	46.4978	1.98	16.24%	0.8020
FOPI: 500 g	48.4998	1.96	21.24%	2.8854

6.2. Second Experiment: Using Control Specifications  $\phi_m = 60^\circ$  and  $\omega_{gc} = 5$  rad/s

Now, a faster performance speed is required and the gain crossover frequency is increased up to  $\omega_{gc} = 5$  rad/s. The Bode plots of the open loop systems with the corresponding PI and FOPI controllers are shown in Figure 11 for the PI case and Figure 12 for the FOPI case.

As can be seen, the phase margin and gain crossover frequency specifications are met in all the cases, and again, the robustness (iso-damping) constraint is fulfilled for the FOPI case. The phase margin for frequencies close to  $\omega_{gc}$  drops rapidly to the instability

region for the PI case, whereas the specified margin is maintained over a wider range of frequencies for the FOPI case.

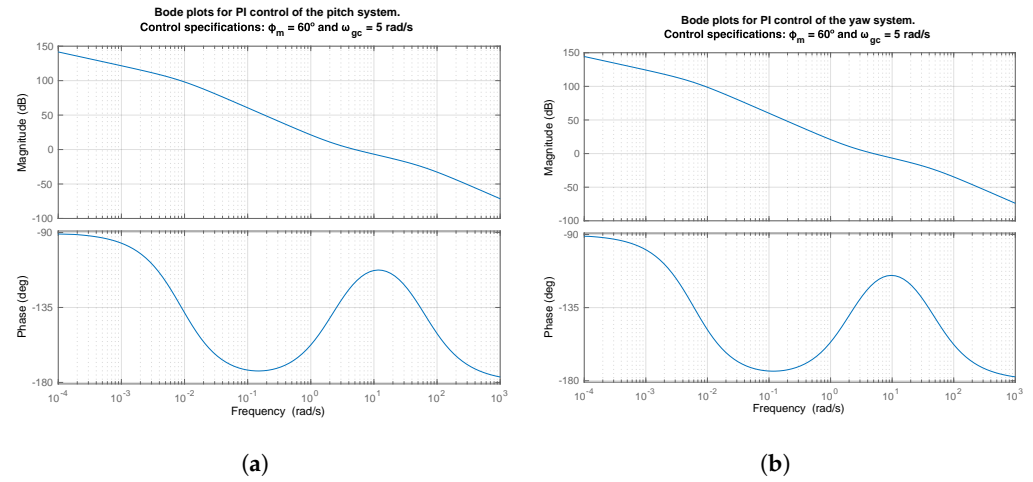


**Figure 11.** Bode plots of the open loop systems with the resulting PI controllers. Control specifications:  $\phi_m = 60^\circ$  and  $\omega_{gc} = 5$  rad/s. (a) Bode plots of the open loop system with the PI controller corresponding to the pitch system. (b) Bode plots of the open loop system with the PI controller corresponding to the yaw system.

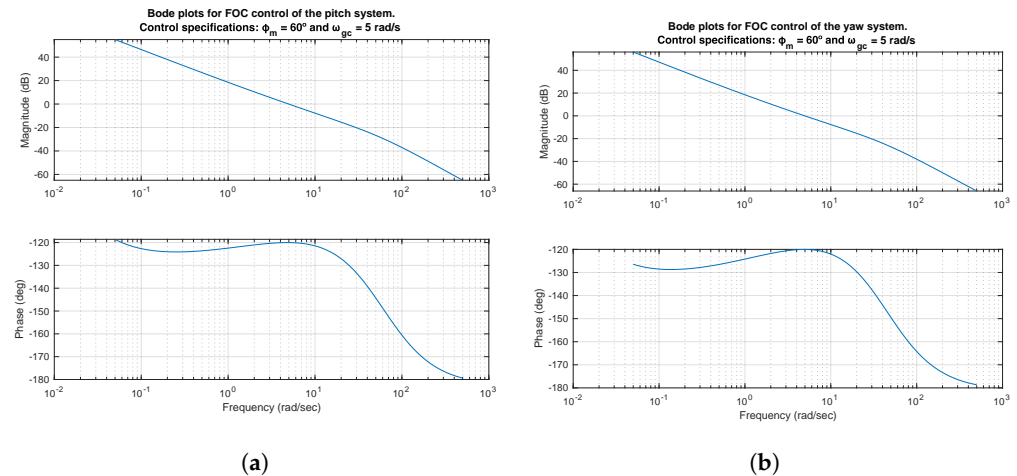


**Figure 12.** Bode plots of the open loop systems with the resulting FOPI controllers. Control specifications:  $\phi_m = 60^\circ$  and  $\omega_{gc} = 5$  rad/s. (a) Bode plots of the open loop system with the FOPI controller corresponding to the pitch system. (b) Bode plots of the open loop system with the FOPI controller corresponding to the yaw system.

In order to test the system performance, an input reference has been selected for the soft arm tip involving both pitch and yaw components. The trajectory is based on a slight modification of the lemniscate of Bernoulli, with  $\alpha$  and  $\beta$  following the next parametric equations:

$$\alpha = \frac{(d\sqrt{2}\cos(nt))}{2(\sin(nt)^2 + 1)} \tag{31}$$

$$\beta = \frac{(d\sqrt{2}\cos(nt)\sin(nt))}{(\sin(nt)^2 + 1)} \tag{32}$$

where  $d$  is the distance from the focus to the origin and  $nt$  is the angle of the focal ratio varying by steps of 0.005 radians at a frequency of 50 Hz.

Figure 13 shows the time response of the system for the PI and FOPI cases with no load at the tip. It can be seen that both controllers perform correctly and the arm tracks the reference quite accurately.

There are three trajectory points where the arm tip is observed to slightly move away from the reference: around  $[-22, 2]$ ,  $[-5, -11]$  and  $[5, -11]$ , where the first coordinate corresponds to the yaw angle and the second to the pitch. This is not due to the control but to the mechanical nature of the arm and its constant curvature, which forces winding and unwinding changes of the tendons when different movement regions are reached in order to correctly track the reference.

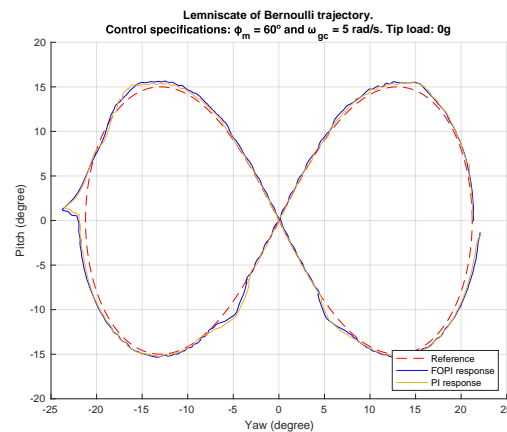


**Figure 13.** PI and FOPI system response to a lemniscate of Bernoulli input reference. Control specifications:  $\phi_m = 60^\circ$  and  $\omega_{gc} = 5$  rad/s. Tip load: 0 g.

When the same test is performed with a disc of 500 g placed at the arm tip, the system shows the response of Figure 14. The presence of load makes the PI system unable to track the reference in three of the four movement regions, and very significant oscillations are observed. However, a better performance is fulfilled for the FOPI case, where model mismatches caused by the mass are robustly faced, allowing much more accurate reference tracking and ensuring the system stability. Only slight oscillations appear in some parts of the trajectory, which could be reduced from the design stage by selecting the adequate elasticity of the soft material according to the loads to be managed.

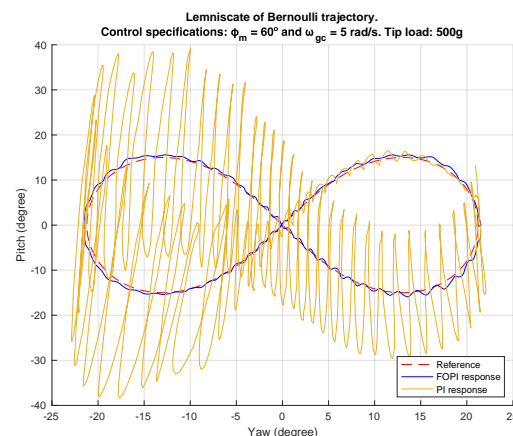


**Figure 14.** PI and FOPI system response to a lemniscate of Bernoulli input reference. Control specifications:  $\phi_m = 60^\circ$  and  $\omega_{gc} = 5$  rad/s. Tip load: 500 g.

Table 7 shows the RMSE values both for pitch and yaw trajectory components for the PI and FOPI controllers with and without load. It can be observed that, in comparison with the RMS values obtained from the first experiment, where a step trajectory was selected, the

tracking error in this second experiment has been reduced. As expected, the PI performance with the 500 g load shows the worst results (more affected by the influence of gravity), whereas the FOPI performance is remarkable.

**Table 7.** RMSE of controllers designed with  $\phi_m = 60^\circ$  and  $\omega_{gc} = 5$  rad/s.

Trajectory Component	FOPI: 0 g	PI: 0 g	FOPI: 500 g	PI: 500 g
Pitch	0.8576	0.7357	0.6749	11.5717
Yaw	0.4862	0.4556	0.2271	0.6521

In order to assess the system behavior when a more demanding reference is used, Figure 15 shows the PI and FOPI responses to a step input of  $\alpha = 40^\circ$  and  $\beta = 0^\circ$  for the 500 g load case. The PI system shows a limit cycle performance, whereas the FOPI response is far from instability.

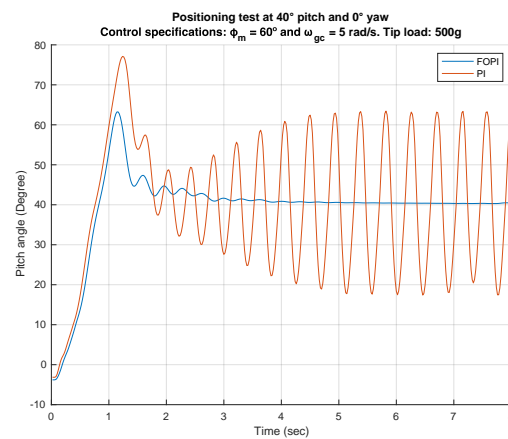


**Figure 15.** FOPI and PI controller ( $\phi_m = 60^\circ$  and  $\omega_{gc} = 5$  rad/s) response to  $\alpha = 40^\circ$  and  $\beta = 0^\circ$  with 500 g mass at the end.

From the tests, the difficulties that arise when controlling soft robots can be appreciated. Working with masses or velocities causes the nonlinearities of the system to show up, demonstrating a performance that is difficult to handle and predict. It has been observed that for tasks without loads or where the soft body movement does not have to be fast, both PI and FOPI work properly. However, when a faster response is needed, and when loads are involved, the PI controller is not able to perform correctly, while the FOPI manages to perform much more robustly.

A video of the experimental results discussed in this section for the case of the robot supporting a load of 500 g (worst case) can be seen here: <https://vimeo.com/762360018> (accessed on 15 December 2022).

## 7. Conclusions

The soft arm presented is a complex platform where new problems arise that require methodologies to be used in real environments with precision. Due to deformations and nonlinearities, these platforms are difficult to model and control. This work addresses this challenge for the first time for this robotic platform.

Several conclusions can be drawn from the results presented in this paper. First of all, satisfactory results have been obtained from the system identification based on two decoupled transfer functions that accurately model the response of the arm. Second, different controllers have been developed and a comparison has been made between them based on tests such as the tracking of a trajectory with the shape of the Lemniscate curve and the performance when a load is connected to the arm tip.

In this work, controllers have been designed with the following specifications:  $\phi_m = 60^\circ$  and  $\omega_{gc} = 1.5$  rad/s. PI controllers are proposed and show stable responses when acting under load, and this is also fulfilled by the FOPI controller. However, the challenge of soft robot control lies in performing tasks with faster responses. This is the reason why tests with specifications  $\phi_m = 60^\circ$  and  $\omega_{gc} = 5$  rad/s have been carried out. In this case, the PI controller that had previously been able to perform the control correctly encounters difficulties in performing load management, not following the reference and showing an oscillatory behavior. As a novel solution for this robot, the use of the FOPI controller shows stable and robust performance, being able to perform the task demanded of the soft arm correctly.

Future works will deal with the use of machine learning techniques for the modeling and control of the soft arm in order to study how they compare with these analytical approaches.

**Author Contributions:** Conceptualization, C.R., J.M., C.A.M., S.M. and D.G.; methodology, C.R., J.M., C.A.M., S.M. and D.G.; software, C.R. and J.M.; validation, C.R. and J.M.; formal analysis, C.R., J.M., C.A.M., S.M. and D.G.; investigation, C.R., J.M., C.A.M., S.M. and D.G.; resources, C.A.M., S.M. and D.G.; data curation, C.R. and J.M.; writing—original draft preparation, C.R. and J.M.; writing—review and editing, C.A.M., S.M. and D.G.; visualization, C.R. and J.M.; supervision, C.A.M., S.M. and D.G.; project administration, C.A.M.; funding acquisition, C.A.M., S.M. and D.G. All authors have read and agreed to the published version of the manuscript.

**Funding:** This research has been supported by the project SOFIA, with reference PID2020-113194GB-I00, funded by the Spanish Ministry of Economics, Industry and Competitiveness, and the project Desarrollo de articulaciones blandas para aplicaciones robóticas, with reference IND2020/IND-1739, funded by the Comunidad Autónoma de Madrid (CAM) (Department of Education and Research).

**Data Availability Statement:** Not applicable.

**Conflicts of Interest:** The authors declare no conflict of interest.

## References

1. Bruder, D.; Gillespie, B.; Remy, C.D.; Vasudevan, R. Modeling and control of soft robots using the koopman operator and model predictive control. *arXiv* **2019**, arXiv:1902.02827.
2. George Thuruthel, T.; Ansari, Y.; Falotico, E.; Laschi, C. Control strategies for soft robotic manipulators: A survey. *Soft Robot.* **2018**, *5*, 149–163. [[CrossRef](#)] [[PubMed](#)]
3. Duriez, C. Control of elastic soft robots based on real-time finite element method. In Proceedings of the 2013 IEEE International Conference on Robotics and Automation, Karlsruhe, Germany, 6–10 May 2013; pp. 3982–3987.
4. Rus, D.; Tolley, M.T. Design, fabrication and control of soft robots. *Nature* **2015**, *521*, 467–475. [[CrossRef](#)] [[PubMed](#)]
5. Lee, C.; Kim, M.; Kim, Y.J.; Hong, N.; Ryu, S.; Kim, H.J.; Kim, S. Soft robot review. *Int. J. Control Autom. Syst.* **2017**, *15*, 3–15. [[CrossRef](#)]
6. Coevoet, E.; Escande, A.; Duriez, C. Soft robots locomotion and manipulation control using FEM simulation and quadratic programming. In Proceedings of the 2019 2nd IEEE International Conference on Soft Robotics (RoboSoft), Seoul, Republic of Korea, 14–18 April 2019; pp. 739–745.
7. Polygerinos, P.; Wang, Z.; Overvelde, J.T.; Galloway, K.C.; Wood, R.J.; Bertoldi, K.; Walsh, C.J. Modeling of soft fiber-reinforced bending actuators. *IEEE Trans. Robot.* **2015**, *31*, 778–789. [[CrossRef](#)]
8. Gisby, T.A.; O'Brien, B.M.; Anderson, I.A. Self sensing feedback for dielectric elastomer actuators. *Appl. Phys. Lett.* **2013**, *102*, 193703. [[CrossRef](#)]
9. Tang, X.; Li, K.; Chen, W.; Zhou, D.; Liu, S.; Zhao, J.; Liu, Y. Temperature self-sensing and closed-loop position control of twisted and coiled actuator. *Sens. Actuators A Phys.* **2019**, *285*, 319–328. [[CrossRef](#)]
10. Lan, C.C.; Fan, C.H. An accurate self-sensing method for the control of shape memory alloy actuated flexures. *Sens. Actuators A Phys.* **2010**, *163*, 323–332. [[CrossRef](#)]
11. Best, C.M.; Gillespie, M.T.; Hyatt, P.; Rupert, L.; Sherrod, V.; Killpack, M.D. A new soft robot control method: Using model predictive control for a pneumatically actuated humanoid. *IEEE Robot. Autom. Mag.* **2016**, *23*, 75–84. [[CrossRef](#)]
12. Renda, F.; Giorelli, M.; Calisti, M.; Cianchetti, M.; Laschi, C. Dynamic model of a multibending soft robot arm driven by cables. *IEEE Trans. Robot.* **2014**, *30*, 1109–1122. [[CrossRef](#)]
13. Muñoz, J.; Copaci, D.S.; Monje, C.A.; Blanco, D.; Balaguer, C. Iso-m based adaptive fractional order control with application to a soft robotic neck. *IEEE Access* **2020**, *8*, 198964–198976. [[CrossRef](#)]
14. Shah, P.; Agashe, S. Review of fractional PID controller. *Mechatronics* **2016**, *38*, 29–41. [[CrossRef](#)]

15. Monje, C.A.; Chen, Y.; Vinagre, B.M.; Xue, D.; Feliu-Batlle, V. *Fractional-Order Systems and Controls: Fundamentals and Applications*; Springer Science & Business Media: Berlin/Heidelberg, Germany, 2010.
16. Muñoz, J.; Piqué, F.; A Monje, C.; Falotico, E. Robust Fractional-Order Control Using a Decoupled Pitch and Roll Actuation Strategy for the I-Support Soft Robot. *Mathematics* **2021**, *9*, 702. [[CrossRef](#)]
17. Deutschmann, B.; Ott, C.; Monje, C.A.; Balaguer, C. Robust motion control of a soft robotic system using fractional order control. In *Proceedings of the International Conference on Robotics in Alpe-Adria Danube Region*; Springer: Berlin/Heidelberg, Germany, 2017; pp. 147–155.
18. Nagua, L.; Relaño, C.; Monje, C.A.; Balaguer, C. A New Approach of Soft Joint Based on a Cable-Driven Parallel Mechanism for Robotic Applications. *Mathematics* **2021**, *9*, 1468. [[CrossRef](#)]
19. Monje, C.A.; Relaño, C.; Nagua, L.F.; Martínez de la Casa, S.; Balaguer, C. Link for Soft Joint and Soft Joint Comprising the Link. WO2022013469A1. Available online: <https://patents.google.com/patent/WO2022013469A1/en> (accessed on 15 December 2022).
20. Åström, K.J.; Hägglund, T.; Astrom, K.J. *Advanced PID Control*; ISA-The Instrumentation, Systems, and Automation Society Research Triangle Park: Pittsburgh, PA, USA, 2006; Volume 461.
21. Nagua, L.; Monje, C.; Yañez-Barnuevo, J.M.; Balaguer, C. Design and performance validation of a cable-driven soft robotic neck. In *Proceedings of the Proc. Actas de las Jornadas Nacionales de Robótica*, Valladolid, Spain, 14–15 June 2018; pp. 1–5.
22. Park, Y.J.; Huh, T.M.; Park, D.; Cho, K.J. Design of a variable-stiffness flapping mechanism for maximizing the thrust of a bio-inspired underwater robot. *Bioinspir. Biomim.* **2014**, *9*, 036002. [[CrossRef](#)] [[PubMed](#)]
23. Webster III, R.J.; Jones, B.A. Design and kinematic modeling of constant curvature continuum robots: A review. *Int. J. Robot. Res.* **2010**, *29*, 1661–1683. [[CrossRef](#)]
24. Young, P.; Jakeman, A. Refined instrumental variable methods of recursive time-series analysis Part III. Extensions. *Int. J. Control* **1980**, *31*, 741–764. [[CrossRef](#)]
25. Ozdemir, A.A.; Gumussoy, S. Transfer function estimation in system identification toolbox via vector fitting. *IFAC-PapersOnLine* **2017**, *50*, 6232–6237. [[CrossRef](#)]
26. Åström, K.J.; Hägglund, T. *Control PID Avanzado*; Pearson: Madrid, Spain, 2009.
27. Borase, R.P.; Maghade, D.; Sondkar, S.; Pawar, S. A review of PID control, tuning methods and applications. *Int. J. Dyn. Control* **2021**, *9*, 818–827. [[CrossRef](#)]
28. Li, Y.; Ang, K.H.; Chong, G.C. PID control system analysis and design. *IEEE Control Syst. Mag.* **2006**, *26*, 32–41.
29. Podlubny, I. Fractional-order systems and PI/sup/spl lambda//D/sup/spl mu//-controllers. *IEEE Trans. Autom. Control* **1999**, *44*, 208–214. [[CrossRef](#)]
30. Monje, C.A.; Vinagre, B.M.; Feliu, V.; Chen, Y. Tuning and Auto-tuning of Fractional Order Controllers for Industry Applications. *Control Eng. Pract.* **2008**, *16*, 798–812. [[CrossRef](#)]
31. Muresan, C.I. Simplified optimization routine for tuning robust fractional order controllers. *Am. J. Comput. Math.* **2013**, *3*, 7–12. [[CrossRef](#)]
32. Levy, E. Complex-curve fitting. *IRE Trans. Autom. Control* **1959**, *AC-4*, 37–43. [[CrossRef](#)]
33. Valério, D.; Da Costa, J.S. *An Introduction to Fractional Control*; IET: London, UK, 2013; Volume 91.

**Disclaimer/Publisher’s Note:** The statements, opinions and data contained in all publications are solely those of the individual author(s) and contributor(s) and not of MDPI and/or the editor(s). MDPI and/or the editor(s) disclaim responsibility for any injury to people or property resulting from any ideas, methods, instructions or products referred to in the content.